This article has been accepted for publication in a future issue of this journal, but has not been fully edited. Content may change prior to final publication. Citation information: DOI10.1109/TAP.2022.3161280, IEEE Transactions on Antennas and Propagation

A Compact Dual-Polarized Filtering Antenna with Steep Cut-Off for Base-Station Applications

Xuekang Liu, Steven Gao, Wei Hu, Lehu Wen, Qi Luo, Benito Sanz-Izquierdo, Xiaodong Chen, Long Qian, Josaphat Tetuko Sri Sumantyo and Xue-Xia Yang

***Abstract*— A dual-polarized filtering antenna with steep cut-off and compact size is developed for base station applications. In this design, four controllable radiation nulls are obtained by utilizing split rings, slotted T-shaped branches, a single-stub tuner, and a parasitic loop. Split rings are firstly used as the dipole arms to obtain the 1st radiation null at upper out-of-band. Four T-shaped branches working as DGS are printed under the crossed dipoles to achieve the 2nd radiation null. The connected outer conductors of the differential feed structure acting as a single-stub tuner can provide the 3rd radiation null to further enhance the upper-band rejection. Finally, a parasitic loop is incorporated around the split rings, and the out-of-band rejection of the lower-band is further enhanced by the 4th radiation null. More importantly, the impedance bandwidth of the antenna can be expended with two newly introduced resonant modes. As a result, a compact filtering antenna with a wide operational bandwidth of 1.7- 3.01 GHz (56%) is realized for $|S_{dd11}|$ < -15 dB with the isolation higher than 38 dB. The out-of-band suppression is higher than 18.4 dB in 3.1-4.5 GHz and more than 47 dB in 0.8-1.1 GHz.**

***Index Terms*— Base station antenna, dual-polarized antenna, steep cut-off, filtering antenna.**

I. Introduction

With the increasing demand for highly integrated base station antennas, subarrays working at different frequency bands need to be arranged in a small shared space. The interferences between antennas have a serious impact on their input impedances and radiation patterns. To solve this problem, some methods have been presented, such as introducing decoupling network, introducing decoupling branches, and using filtering antenna elements [1]-[3].

A decoupling network can be introduced and efficiently minimize the mutual coupling between two antennas by establishing a proper coupling coefficient between two pairs of coupled resonators [1]. However, this type of decoupling approach will degrade the antenna gain, efficiency, and radiation patterns to some extent. In [2], decoupling branches were introduced between the antenna elements to obtain high isolation. However, its large size makes them unsuitable for highly integrated base stations. Apart from the approaches mentioned above, utilizing a filtering element to reduce mutual coupling between antennas is another good option. Thanks to the advantage of good out-of-band suppression, an array antenna with high isolation is proposed in [3] without additional decoupling structures. Compared to the other two methods, the use of filtering antennas can keep a compact size, which is very suitable for base station applications.

For base station applications, antennas are required to be dual-polarized. The commonly used dual-polarized antennas are patch antennas [4]-[5], magneto-electric (ME) dipoles [6]-[7], and crossed dipoles [8]-[13]. A differentially fed dual-polarized antenna with a wide bandwidth of 49.4% was presented in [4] by stimulating the stacked patches with adjustable slots. By feeding the crossed dipoles with an integrated six-port power divider [8], a differentially fed dual-polarized antenna was presented with a wide bandwidth of 58.6% and high common-mode suppression. However, no appealing out-of-band suppression can be achieved in these designs.

There are a variety of ways to get a high suppression level [14]-[20]. By using parasitic components, dual-polarized filtering antennas were designed in [14]-[15]. The currents on the parasitic structures are opposite to the currents on the crossed dipoles. As a result, radiation nulls can be obtained to achieve out-of-band suppression. In [18], by introducing inductors and capacitors, two dual-polarized antennas with improved out-of-band rejection level were realized. In these designs, the rejection band is narrow and they cannot meet the wideband requirements of modern base stations.

In this communication, a wideband and compact dual-polarized filtering antenna with sharp cut-off is proposed for base station applications. The feature of the presented antenna is the steep cut-off for interference suppression, which is realized by four controllable radiation nulls located at the lower and upper out-of-bands. The radiation nulls at higher stopband are realized by the using of split rings, T-shaped branches, and single- stub tuner. The radiation null at lower stopband can be controlled by the parasitic loop. Therefore, a compact wideband dual-polarized antenna with high out-of-band rejection is developed, fabricated, and finally measured for performance verification. Owing to the elaborately introduced radiation nulls, the presented antenna can have a high out-of-band suppression of 47 dB over 0.8-1.1 GHz and 18.4 dB over 3.1-4.5 GHz. Besides, at upper out-of-band, the proposed antenna achieves a sharp.

II. Antenna Configuration

As shown in Fig. 1(a), the proposed filtering antenna is composed of radiator, four coaxial cables, and a reflector with the size of 140mm×140mm. The radiator and the reflector are printed on two Rogers 4003 substrates with the relative dielectric permittivity of 3.55 and thickness of 0.813 mm. Detailed radiator layout is shown in Fig. 1(b). The antenna is designed for ± 45° polarized radiation. It consists of two dipoles, a circular ground patch and a parasitic loop. The parasitic loop and two orthogonal arranged dipoles with split-ring-shaped arms are arranged on the upper layer of substrate 1. Four T-shaped branches with slots working as DGS are connected to the circular patch on the lower layer of substrate 1. To excite the antenna, two pairs of differential signals are excited to the antenna via four coaxial cables. As shown in Fig. 1(c), the inner conductors of the coaxial cables connect to the dipoles on the upper layer of substrate 1, while outer connectors connect the circular patch on the lower layer of substrate 1 to the bottom reflector. The differentially driven S-parameters of the proposed antenna are given as:

This work was supported in part by China Scholarship Council, in part by Huawei Technologies Ltd, and in part by EPSRC under Grant EP/S005625/1. *(Corresponding author: Xuekang Liu.)*

Xuekang Liu, Steven. Gao, Lehu Wen, and Benito Sanz-Izquierdo are with the School of Engineering and Digital Arts, University of Kent, Canterbury CT2 7NT, U.K. (e-mail: xl255@kent.ac.uk).

Wei. Hu is with National Laboratory of Science and Technology on Antennas and Microwaves, Xidian University, Xi'an, Shaanxi 710071, China.

Qi. Luo is with the School of Physics, Engineering and Computer Science, University of Hertfordshire, Hatfield AL10 9AB, U.K.

Xiaodong Chen and Long Qian are with the School of Electronic Engineering and Computer Science, Queen Marry University of London, E1 4NS, UK

Josaphat Tetuko Sri Sumantyo is with the Center for Environmental Remote Sensing, Chiba University, Chiba 263-8522, Japan.

Xue-Xia Yang is with the School of Communication and Information Engineering, Shanghai University, Shanghai 200444, China.

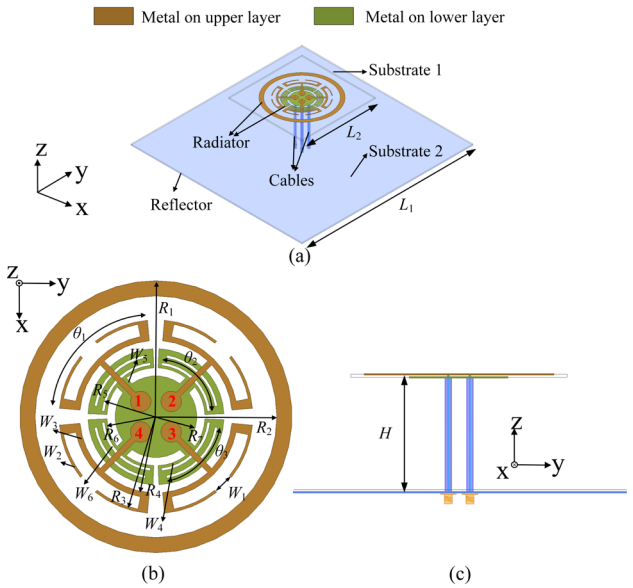

Fig. 1. Configuration of the proposed antenna. (a) 3D view. (b) top view. (c) side view. Dimensions are L_1 = 140, L_2 = 60, W_1 = 3.8, W_2 = 0.5, W_3 = 1, W_4 = 0.5, W_5 = 2.4, W_6 = 1, R_1 = 25, R_2 = 22.2, R_3 = 17.3, R_4 = 14, R_5 = 10.5, R_6 = 9, R_7 = 7.5, H = 34, θ_1 = 80°, θ_2 = 78°, and θ_3 = 70° (unit: millimeter).

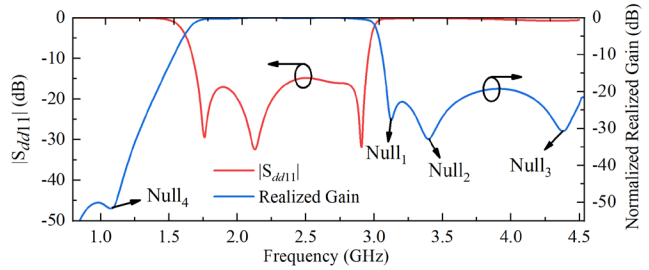

Fig. 2. Simulated $|S_{dd11}|$ and normalized realized gain of the proposed antenna.

$$S_{dd11} = (S_{11} + S_{33} - S_{13} - S_{31})/2 \quad (1)$$

$$S_{dd22} = (S_{22} + S_{44} - S_{24} - S_{42})/2 \quad (2)$$

$$S_{dd21} = (S_{21} + S_{43} - S_{23} - S_{41})/2 \quad (3)$$

$$S_{dd12} = (S_{12} + S_{34} - S_{14} - S_{32})/2 \quad (4)$$

where S_{ij} (i = 1, 2, 3, 4; j = 1, 2, 3, 4) are the single-ended S-parameters. The proposed antenna is simulated using the ANSYS High Frequency Structure Simulator (HFSS) to derive the impedance and radiation performances.

III. Filtering Antenna Design

The simulated $|S_{dd11}|$ and normalized realized gain of the proposed antenna are shown in Fig.2. As can be seen in the figure, four radiation nulls are achieved in both the lower and upper out-of-bands. In detail, by elaborately stimulating four resonant modes, a wide impedance bandwidth for $|S_{dd11}|$ < -15 dB is achieved to cover all the frequency bands of 2G/3G/LTE communication systems. To obtain a good rejection level beside the operating band, four controllable radiation nulls are further introduced by using split rings, slotted T-shaped branches, single-stub tuner, and parasitic loop. The operating principle of each radiation null will be interpreted and validated in detail in the following sub-sections.

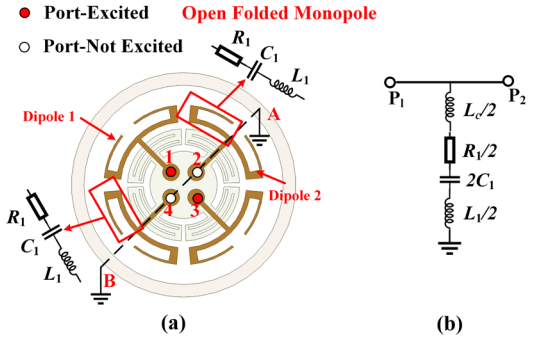

Fig. 3. Equivalent circuit of (a) open folded monopole, and (b) corresponding band stop filter.

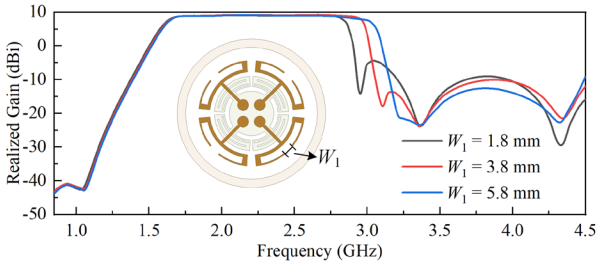

Fig. 4. Simulated realized gains of the proposed antenna under different W_1.

A. The 1st Radiation Null

Here, split-ring dipole arms are firstly utilized for the introduction of the 1st radiation null. Unlike traditional crossed-dipoles, the arms of the dipoles are replaced by split rings in this design to form a band-stop structure.

To interpret the working principle of the 1st radiation null, an equivalent circuit model for the proposed antenna is shown in Fig. 3. Owing to the differentially fed method, the symmetrical plane (A-B) can be equivalent as a virtual ground [21] at the middle of Dipole 2. Due to the symmetry, only a half of the antenna is analyzed. The split rings on Dipole 2 can be divided into two open folded monopoles [22]. Each open folded monopole can be equivalent as a series *R-L-C* resonator. The magnetic coupling [23] between Dipole 1 and open folded monopoles is denoted by a mutual inductance (L_c). Thus, a distributed band stop filter can be obtained, as shown in Fig. 3(b). Due to the low resistance of open folded monopoles [22], the input impedance of the band stop filter (Z_{in}) can be calculated by using:

$$Z_{in} = \frac{j\omega L_c}{2} + \frac{1}{j\omega 2C_1} + \frac{j\omega L_1}{2} \quad (5)$$

The transmission coefficient of the two-port network can be calculated by [23]:

$$S_{21} = 1/(1 + Z_0/2Z_{in}) \quad (6)$$

It can be observed that when $S_{21} = 0$, there will be a transmission zero occurs at:

$$f_{null,1} = \frac{1}{2\pi\sqrt{(L_c + L_1)C_1}} \quad (7)$$

Although the coupling between the crossed dipoles makes the split rings of Dipole 2 resonant at 3.1 GHz, the electromagnetic energy will not be transmitted into port 2 or 4. This is because that when port 1

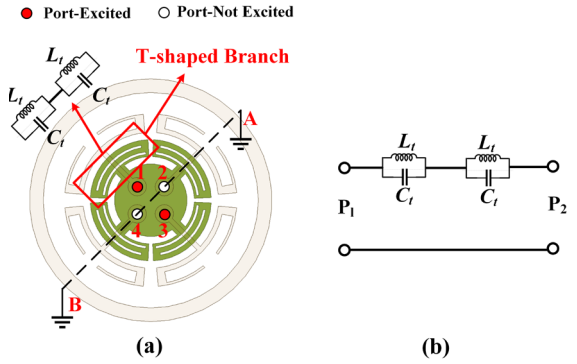

Fig. 5. Equivalent circuit of (a) T-shaped branch, and (b) its corresponding two-port network.

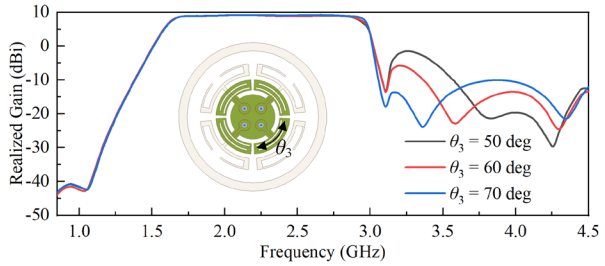

Fig. 6. Simulated realized gains of the proposed antenna under different θ_3.

and 3 are excited by a pair of differential signals, the A-B plane can be equivalent to an electric wall. When Dipole 2 is excited, the A-B plane is equivalent to a magnetic wall. The current distributions of the antenna under these two working statuses are orthogonal. Thus, the resonant modes of Dipole 2 will be suppressed. Therefore, high isolation can be maintained for the presented antenna.

Fig. 4 shows the effect of the different widths of the gap (W_1) on the simulated realized gain of the proposed antenna. When W_1 changes from 1.8 mm to 5.8 mm, the radiation null shifts from 2.9 GHz to 3.3 GHz, while others are nearly unchanged. When W_1 = 3.8 mm, the 1st radiation null appears at 3.1 GHz. It is shown that the first radiation null can be elaborately adjusted, which is critical for the design of a filtering antenna.

B. The 2nd Radiation Null

By etching slots on the T-shaped branches that are under the arms of the crossed dipoles, DGS can be obtained to realize good out-of-band rejection. To the best knowledge of the authors, this is the first time we elaborately insert a DGS structure under the dipole arm in base-station antennas, particularly operating in 1.7-2.7 GHz. In the previously presented designs, DGSs usually be used in the low-profile designs. Such as the microstrip line or the microstrip patch antenna. In these cases, the closely placed DGS structures can perturb the current distribution under the microstrip line and microstrip patch at certain frequency to obtain the transmission zero or the radiation null.

In the common design of base station antenna, especially operating at 1.7-2.7 GHz, the ground/reflector is placed about $\lambda_0/4$ (λ_0 represents the wavelength at central frequency in free space) away from the radiator to maintain stable radiation performance in such a wide bandwidth. Thus, DGS structure is rarely used in the design of dual-polarized base station antenna, especially being integrated in the radiator. Besides, DGS structure will cause the backside radiation issues [24]. This is unacceptable in the design of base station antenna.

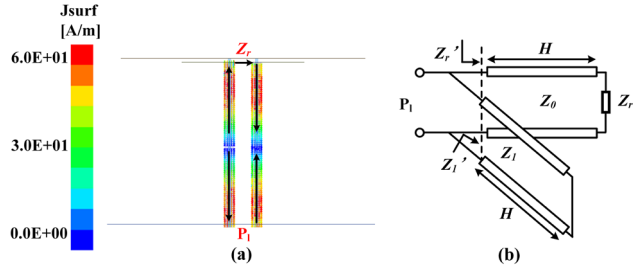

Fig. 7. (a) simulated current distribution on the outer conductor of coaxial tables at 4.4 GHz, (b) equivalent circuit model for the antenna.

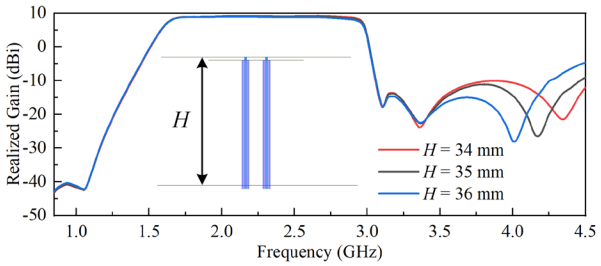

Fig. 8. Simulated realized gains of the proposed antenna under different *H*.

These reasons make DGS difficult to be applied in wideband base station designs.

To overcome these problems, the outer conductors of the coaxial cables are connected together, and elaborately extended to form DGS structures in our design. In this configuration, there are two ground planes/reflectors connected by the out conductors of the cables. The DGS structures are etched on the smaller ground plane/reflector to introduce a radiation null. The larger ground plane/reflector plays an important role in maintaining the radiation performance of the proposed antenna.

An equivalent circuit for the proposed antenna is shown in Fig. 5 to explain the working principle of T-shaped branches. Due to the symmetry, only a half of the antenna is analyzed. As explained in [25], the proposed structure can be equivalent as a parallel inductor (L_t)-capacitor (C_t) circuit. There will be an attenuation pole at the resonant frequency of the parallel *LC* resonator. Thus, the 2nd radiation null occurs at:

$$f_{null,2} = \frac{1}{2\pi\sqrt{L_t C_t}} \tag{8}$$

Fig. 6 shows the simulated peak gains of the proposed antenna under different slot lengths (θ_3). The frequency of the radiation null can be easily adjusted by changing the length of the slot on the T-shaped branches. When the length of the slots become smaller, the frequency of the 2nd radiation null will shift substantially towards higher frequency. Therefore, by adjusting the slots on the T-shaped branches under the crossed dipoles, the 2nd radiation null can be shifted close to the 1st radiation null. Thus, the upper out-of-band rejection can be further enhanced.

C. The 3rd Radiation Null

The 3rd radiation null is introduced at 4.4 GHz by utilizing a single-stub tuner to suppress the out-of-band radiation. The simulated current distribution on the outer conductors of the coaxial cables is shown in Fig. 7(a). The currents on these two cables have same magnitude but with 180-degree phase difference. As shown in Fig. 7(b), at this

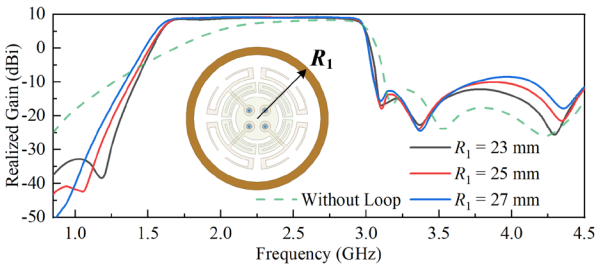

Fig. 9. Simulated realized gains of the proposed antenna under the effect of parasitic loop.

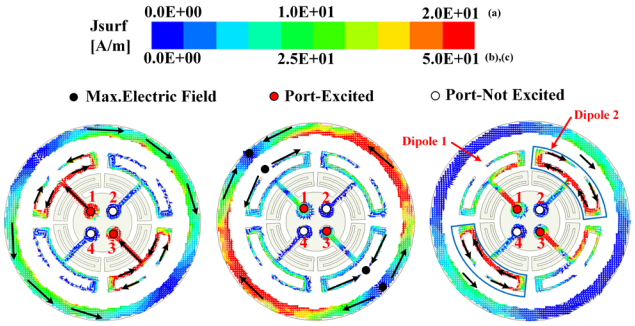

Fig. 10. Simulated current vector distribution of the proposed antenna at (a) 1.1 GHz, (b) 1.8 GHz, and (c) 2.9 GHz.

frequency, the outer conductors of the differential coaxial cables can be seen as two-wire transmission line with shorted ends and length H (H is the height of the antenna). Thus, the input impedance of the antenna can be written as:

$$Z_{in} = Z_1' // Z_r' \tag{9}$$

Z_1' and Z_r' can be expressed as:

$$Z_1' = jZ_1 tan\beta H \tag{10}$$

$$Z_r' = Z_0 \frac{Z_0 + jZ_r tan\beta H}{Z_r + jZ_0 tan\beta H} \tag{11}$$

where Z_0 is the characteristic impedance of the coaxial cable. Z_1 is the characteristic impedance of the two-wire transmission line. Z_r is the radiation resistance of the antenna. β is the wave number. H is the height of the antenna. It is obviously that when $H = \lambda/2$, Z_1' will be 0. Thus, there will be a radiation null at:

$$f_{null,3} = \frac{c}{2H} \tag{12}$$

Fig. 8 gives the simulated peak gains of the proposed antenna under different height H. It can be seen that the frequency of the 3rd radiation null can be easily adjusted by changing the height of the proposed antenna. The 3rd radiation null will shift towards lower frequency band with the increase of H, while other radiation nulls are nearly unchanged.

D. The 4th Radiation Null and Additional Resonant Modes

By introducing three radiation nulls, the upper out-of-band radiation is effectively suppressed. So, the 4th radiation null introduced by the

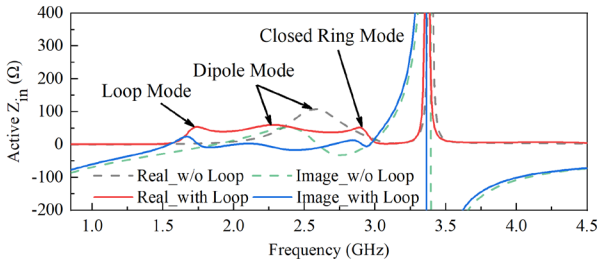

Fig. 11. Simulated input impedance of the proposed antenna with and without parasitic loop.

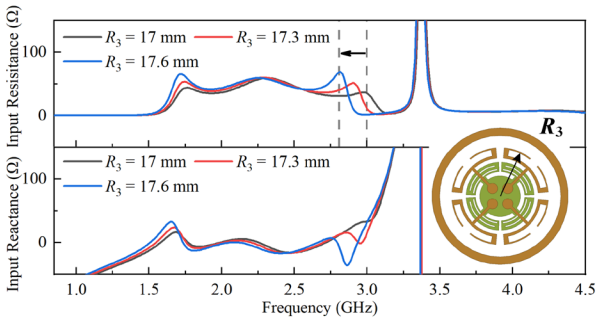

Fig. 12. Simulated input impedance of the proposed antenna under different R_3.

parasitic loop is arranged at 1.1 GHz to enhance the lower out-of-band rejection. Although parasitic structure has also been used in [15] to obtain radiation null at lower out-of-band and introduce new resonance in operating band. The biggest difference in these two structures is that the parasitic loop in our design can introduce one more resonance in the operating band than the parasitic structure in [15]. It is very important for expanding the impedance bandwidth of the proposed antenna.

Fig. 9 depicts the effects of the parasitic loop on the proposed antenna. It can be clearly seen that the realized gain of the proposed antenna drops slowly when without the parasitic loop. The lowest realized gain in lower out-of-band is -25 dBi. After introducing the parasitic loop, the 4th radiation null appears at 1.1 GHz. Its frequency can be conveniently adjusted by changing the outer radius (R_1). As R_1 increase, the 4th radiation null shifts toward a lower frequency without influencing other radiation nulls of the proposed antenna.

The simulated current contribution of the proposed antenna at 1.1 GHz is shown in Fig. 10(a) to demonstrate the resonance of the 4th radiation null. As can be seen, the parasitic loop's current vector is in the opposite direction to the current on the dipole arms. As a result, the coupled current on the parasitic loop cancels the current radiation on the dipole, and a radiation null is achieved.

In addition, the most important part in this design is that two additional resonances can be effectively introduced by using the parasitic loop. Fig. 11 shows the comparison of input impedances between the proposed antenna with and without parasitic loop. It can be clearly seen that two new resonances of loop mode and closed-ring mode are successfully excited at 1.8 GHz and 2.9 GHz.

The simulated current distribution of the first loop mode at 1.8 GHz is given in Fig. 10(b). When the dipole is excited, the currents on the split-rings are in-phase due to the out-of-phase between the two feeding lines. Because of the symmetry of the split rings, a reverse current component at the ends of the arms is observed. Therefore, typical electric coupling [23] is formed between dipole arms and parasitic loop. The currents are coupled from the split-ring arms to the

This article has been accepted for publication in a future issue of this journal, but has not been fully edited. Content may change prior to final publication. Citation information: DOI10.1109/TAP.2022.3161280, IEEE Transactions on Antennas and Propagation

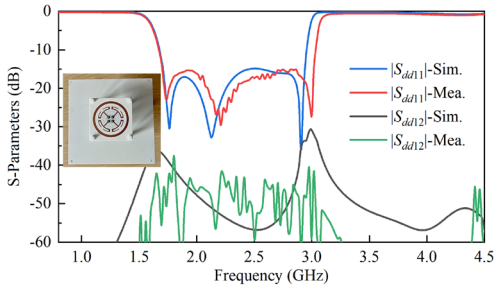

Fig. 13. Measured and simulated S-parameters of the proposed antenna.

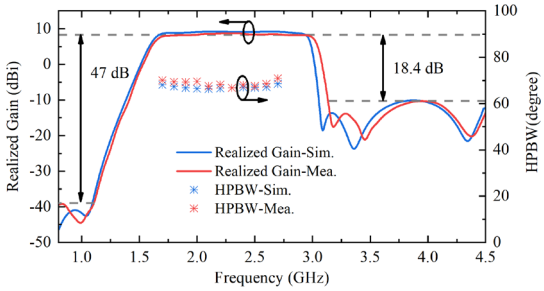

Fig. 14. Measured and simulated realized gains of the proposed antenna.

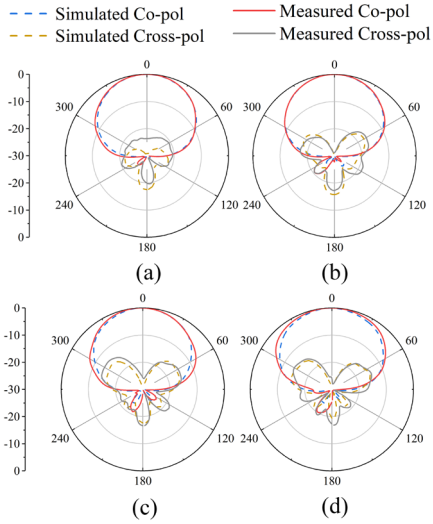

Fig. 15. Measured and simulated normalized radiation patterns of the proposed antenna in horizontal plane at (a) 1.7 GHz, (b) 2.2 GHz, (c) 2.7 GHz, and (d) 2.9 GHz.

parasitic loop through the feeding gap, and the overall current vector on parasitic loop is along -45° direction.

Apart from the loop mode, as shown in Fig. 11, the second closed-ring mode appears at 2.9 GHz after introducing the parasitic loop. At this frequency, due to the coupling between the split rings on Dipole 2 and the parasitic loop, these two structures can be seen as a closed ring. The electromagnetic energy will radiate into the free space through the combined structure of split rings on Dipole 2 and the parasitic loop. Fig. 10(c) depicts the simulated current distribution of the proposed antenna of this closed-ring mode at 2.9 GHz. It can be seen that the current density is concentrated on the parasitic loop and the split rings of Dipole 2.

The closed-ring mode can be independently controlled by changing the radius of the closed-ring R_3. Fig. 12 shows the simulated input impedance of the proposed antenna under different R_3. It can be seen that, with the increase of R_3, the resonant frequency of the closed ring mode shifts from 3.0 GHz to 2.8 GHz with little influence on the other two resonant modes. Therefore, to achieve a wide bandwidth, R_3 = 17.3 mm is chosen in the final design.

TABLE I
COMPARISON OF THE DUAL-POLARIZED FILTERING ANTENNAS

Ref.	BW	Size (mm^2)	Gain (dBi)	*RoR* (dB / GHz)	Ctrl. Nulls	Rej. Level (dB)	Fabrication
[7]	1.58-2.79 (55%)	60×73	7.8;	77; 85	2	17.5; 17	Simple
[14]	1.63-3.05 (61%)	48×48	8.2;	/; 68	2	/; 7.2	Moderate
[15]	1.66-2.73 (49%)	50×50	8.1;	65; 106	2	20.7; 17.3	Complex
* [16]	1.70-2.80 * (49%)	61×61	8.0;	61; 45	2	16.3; 8.5	Simple
*[26]	1.81-3.73 * (69%)	60×60	8.2;	55; 57	3	22.3; 15.7	Simple
Pro.	**1.70-3.01 (56%)**	**50×50**	**8.3;**	**77; 170**	**4**	**47; 18.4**	**Simple**

Ctrl. Nulls and Rej. Level represent controllable nulls and rejection level.
* means the reference level of $|S_{11}|$ is -10 dB.

IV. RESULTS AND DISCUSSION

In this section, to validate design concept, a prototype of the proposed filtering antenna is fabricated and measured. The S-parameters of the proposed antenna were measured by using Rohde&Schwarz ZNBT 8 vector network analyzer at the Queen Mary University of London. The measured far-field results were obtained in the anechoic chamber at the University of Kent. As shown in Fig. 13, the measured and simulated S-parameters are in reasonable agreement with each other. It can be observed from the measured results that the fabricated antenna obtains a wide impedance bandwidth of 56% (1.7 GHz- 3.01 GHz) and good out-of-band rejection with measured $|S_{dd11}|$ > -1 dB in 0.8- 1.5 GHz and 3.1- 4.5 GHz. The isolation between the two differential ports is higher than 38 dB.

Fig. 14 shows the measured and simulated realized gains of the proposed antenna. A stable realized gain of around 8.3 dBi is achieved within the passband. The slight ripples within the bandwidth can be attributed to the introduction of the balun and machining errors. The measured and simulated normalized radiation patterns of the proposed antenna at 1.7 GHz, 2.2 GHz, 2.7 GHz, and 2.9 GHz are given in Fig. 15. Due to the symmetry of the antenna, only horizontal plane (H-plane) radiation patterns are given here. As can be observed, the measured results are in good agreement with the simulated results. The measured half-power beamwidth varies from 67° to 71°. The measured cross-polarization level is 25 dB lower than the co-polarization level in broadside and 16 dB lower within ±30°.

Table I compares the performances of the proposed antenna with the other recently reported dual-polarized filtering antennas. To evaluate the filtering performance of the antennas, roll-off rates of the antennas at both lower and upper band-edges are calculated by using [27]:

$$RoR = \frac{20-3}{|f_{20\,dB} - f_{3\,dB}|} \tag{13}$$

where *RoR* represents roll-off rate, the frequency $f_{3\,dB}$ corresponds to a 3 dB reduction in average realized gain. $f_{20\,dB}$ is the frequency where the average realized gain drops 20 dB or the frequency of the first radiation null.

It can be seen in Table I that the proposed antenna obtains two more controllable nulls than other designs. By etching C-slots on the planar

This article has been accepted for publication in a future issue of this journal, but has not been fully edited. Content may change prior to final publication. Citation information: DOI10.1109/TAP.2022.3161280, IEEE Transactions on Antennas and Propagation

dipole, a filtering antenna with good rejection level is proposed in [7]. However, this antenna has only single polarization, and its size is relatively large. By employing parasitic split rings and modified baluns, a dual-polarized filtering antenna in [14] realizes a wide bandwidth in a compact size. But the upper roll-off rate is too small to effectively suppress the undesired interferences in the adjacent frequency band. Besides, the crossed coaxial baluns are hard to be fabricated. A filtering antenna with a sharp roll-off rate was proposed in [15] by combining parasitic square, parasitic cross loops, and open-ended stubs. Unfortunately, its impedance bandwidth is slightly narrow. In addition, it has three substrate layers and two pair of modified baluns, which is complicated and costly for fabrication. By utilizing inherent resonance modes, a filtering antenna in [16] obtains two controllable radiation nulls with simple structure. However, the rejection level is relatively low. In [26], highpass filter network and integrated lowpass filter network are used to design a wideband filtering antenna. However, its size is relatively large. Besides, the *RoR* is much lower than the presented antenna. Through the above comparison, the developed antenna achieves a wide bandwidth, a sharp *RoR* of 77 dB/GHz and 170 dB/GHz both lower and upper band-edges. Therefore, it is a promising candidate to be applied in nowadays multi-band base station array antenna designs.

V. Conclusion

A new method to design compact dual-polarized filtering antenna is proposed. Four controllable radiation nulls are successfully introduced to realize a high out-of-band rejection. Three radiation nulls at upper out-out-of-band are realized by using split rings, slotted T-shaped branches, and single -stub tuner, respectively. Each radiation null can be adjusted independently by changing its key parameter. To enhance the bandwidth and lower out-of-band rejection, a parasitic loop is incorporated around the crossed-dipole. By introducing the parasitic loop, two additional resonant modes can be excited to expand the impedance bandwidth. The proposed antenna realizes a wide bandwidth of 56% (1.7 GHz -3.01 GHz) with a compact size, and high upper band *RoR* of 170 dB/GHz. Besides, the presented antenna can have a high out-of-band suppression of 47 dB over 0.8-1.1 GHz and 18.4 dB over 3.1-4.5 GHz. To verify the design method, the antenna prototype was fabricated and measured. The measured results agree well with the simulated results. Such a compact, wideband dual-polarized filtering antenna is a promising candidate for multiband base-station applications.

References

[1] L. Y. Zhao, and K. L. Wu "A dual-band coupled resonator decoupling network for two coupled antennas," *IEEE Trans. Antennas Propag.*, vol. 63, no. 7, pp. 2843–2850, Jul. 2015.

[2] H. Q. Zhai, L. Xi, Y. P. Zang, and L. Li, "A low-profile dual-polarized high-isolation MIMO antenna arrays for wideband base-station applications," *IEEE Trans. Antennas Propag*., vol. 66, no. 1, pp. 191–202, Jan. 2018.

[3] M. Li, Q. L. Li, B. Wang, C. F. Zhou, and S. W. Cheung, "A miniaturized dual-band base station array antenna using band notch dipole antenna elements and AMC reflectors," *IEEE Trans. Antennas Propag*., vol. 66, no. 6, pp. 3189–3194, Jun. 2018.

[4] Z. Y. Tang, J. H. Liu, Y. M. Cai, J. H. Wang, and Y. Z. Yin, "A wideband differentially fed dual-polarized stacked patch antenna with tuned slot excitations," *IEEE Trans. Antennas Propag*., vol. 66, no. 4, pp. 2055-2060, Apr. 2018.

[5] Y. Y. Jin, and Z. W. Du, "Broadband dual-polarized F-probe fed stacked patch antenna for base stations," *IEEE Antennas Wireless Propag. Lett.*, vol. 14, pp. 1121-1124, 2015.

[6] B. T. Feng, W. X. An, S. X. Yin, L. Deng and S. F. Li, "Dual-wideband complementary antenna with a dual-layer cross-ME-dipole structure for 2G/3G/LTE/WLAN applications," *IEEE Antennas Wireless Propag. Lett*., vol. 14, pp. 626-629, 2015.

[7] G. Zhang, L. Ge, J. Wang and J. Yang, "Design of a 3-D integrated wideband filtering magneto-electric dipole antenna," *IEEE Access*, vol. 7, pp. 4735-4740, 2019.

[8] L. H. Wen, S. Gao, Q. Luo, W. Hu, Q. L. Yang, Y. Z. Yin, X. F. Ren, and J. Wu, "A wideband differentially driven dual-polarized antenna by using integrated six-port power divider," *IEEE Trans. Antennas Propag*., vol. 67, no. 12, pp. 7252-7260, Dec. 2019.

[9] D. Z. Zheng, and Q. X. Chu, "Wideband dual-polarized antenna with two independently controllable resonant modes and its array for base-station applications," *IEEE Antennas Wireless Propag. Lett.*, vol. 16, pp. 2014-2017, 2017.

[10] S. Martin-anton, and D. Segovia-vargas, "Fully planar dual-polarized broadband antenna for 3G, 4G and Sub 6-GHz 5G base stations," *IEEE Access.*, vol.8, pp. 91940–91947, 2020.

[11] Y. H. Cui, X. N. Gao, and R. L. Li, "A broadband differentially fed dual-polarized planar antenna," *IEEE Trans. Antennas Propag*., vol. 65, no. 6, pp. 3231-3234, Jun. 2017.

[12] Y. H. Cui, X. N. Gao, H. Z. Fu, Q. X. Chu, and R. L. Li, "Broadband dual-polarized dual-dipole planar antennas: analysis, design, and application for base stations," *IEEE Antennas Propag. Mag.,* vol. 59, no. 6, pp. 77–87, Dec. 2017.

[13] R. Wu, and Q. X. Chu, "A wideband dual-polarized antenna for LTE700/GSM850/GSM900 applications," *IEEE Antennas Wireless Propag. Lett*., vol.16, pp. 2098–2101, 2017

[14] L. H. Wen, S. Gao, Q. Luo, Q. L. Yang, W. Hu, Y. Z. Yin, X. F. Ren, and J. Wu, "A compact wideband dual-polarized antenna with enhanced upper out-of-band suppression," *IEEE Trans. Antennas Propag.*, vol. 67, no. 8, pp. 5194-5202, Aug. 2019.

[15] C. F. Ding, X. Y. Zhang, Y. Zhang, Y. M. Pan, Q. Xue, "Compact broadband dual-polarized filtering dipole antenna with high selectivity for base-station applications," *IEEE Trans. Antennas Propag.*, vol. 66, no. 11, pp. 5747–5756, Nov. 2018.

[16] Y. F. Cao, Y. F. Wu, Y. -M. Pan and X. Y. Zhang, "A method of generating radiation nulls utilizing inherent resonance modes for dual-polarized filtering dipole antenna design," *IEEE Trans. Antennas Propag.*, vol. 68, no. 8, pp. 6413-6418, Aug. 2020.

[17] Q. X. Chu, Y. L. Chang, and J. P. Li, "Crisscross-shaped ±45° dual-polarized antenna with enhanced bandwidth for base stations," *IEEE Trans. Antennas Propag*., vol. 69, no. 4, pp. 2341–2346, Apr. 2021.

[18] M. Li, J. M. Yasir, C. F. Zhou, L. J. Jiang, and L. Yeung, "A novel dipole configuration with improved out-of-band rejection and its applications in low-profile dual-band dual-polarized stacked antenna arrays," *IEEE Trans. Antennas Propag*., vol. 69, no. 6, pp. 3517–3522, Jun. 2021.

[19] C-X Mao, S. Gao, Y. Wang, Q. Luo, and Q-X. Chu, "A shared-aperture dual-Band dual-Polarized filtering-antenna-array with improved frequency response," *IEEE Trans. Antennas Propag*., vol. 65, no. 4, pp. 1836–1844, Apr. 2017.

[20] C-X Mao, S. Gao, Y. Wang, F. Qin, and Q-X. Chu, "Multimode resonator-fed dual-polarized antenna array with enhanced bandwidth and selectivity," *IEEE Trans. Antennas Propag*., vol. 63, no. 12, pp. 5492–5499, Dec. 2015.

[21] W. R. Eisenstadt, B. Stengel, and B. M. Thompson, *Microwave Differential Circuit Design Using Mixed-Mode S-Parameters.* Artech, 2006.

[22] Bengt Josephson, "The Quarter-Wave Dipole," *IRE Wescon Conv. Rec.*, part I (August 1957): 77.

[23] J.-S. G. Hong and M. J. Lancaster, *Microstrip Filters for RF/Microwave Applications.* New York, NY, USA: Wiley, 2001.

[24] C. Kumar and D. Guha, "Mitigating backside radiation issues of defected ground structure integrated microstrip patches," *IEEE Antennas Wireless Propag. Lett*., vol. 19, no. 12, pp. 2502-2506, Dec. 2020.

[25] D. Ahn, J. S. Park, C. S. Kim, J. Kim, Y. Qian, and T. Itoh, "A design of the low-pass filter using the novel microstrip defected ground structure," *IEEE Trans. Microw. Theory Techn.*, vol. 49, no. 1, pp. 86–93, Jan. 2001.

[26] Y. Zhang, X. -Y. Zhang and Q. -H. Liu, "Dual-polarized filtering magnetoelectric dipole antenna utilizing intrinsic highpass filter network and integrated lowpass filter network," *IEEE Trans. Antennas Propag*., vol. 69, no. 12, pp. 8090-8099, Dec. 2021.

[27] F.-C. Chen, R.-S. Li, J.-M. Qiu and Q.-X. Chu, "Sharp-rejection wideband bandstop filter using stepped impedance resonators," *IEEE Trans. Compon., Packag., Manuf. Technol.*, vol. 7, no. 3, pp. 444–449, Mar. 2017.